Muon Tomography for Imaging Nuclear Waste and Spent Fuel Verification

G. Jonkmans[1], V. N. P. Anghel[1], M. Thompson[1]
[1] Atomic Energy of Canada Limited, Chalk River Labs, Chalk River, Canada

Abstract

This paper explores the use of cosmic ray muons to image the content of, and to detect high-Z special nuclear material inside, shielded containers. Cosmic ray muons are a naturally occurring form of radiation, are highly penetrating and exhibit large scattering angles on high Z materials. Specifically, we investigated how radiographic and tomographic techniques can be effective for non-invasive nuclear waste characterization and for nuclear material accountancy of spent fuel inside dry storage containers. We show that the tracking of individual muons, as they enter and exit a structure, can potentially improve the accuracy and availability of data on nuclear waste and the content of Dry Storage Containers (DSC) used for spent fuel storage at CANDU® plants. This could be achieved in near real time, with the potential for unattended and remotely monitored operations. We show that the expected sensitivity to perform material accountancy, in the case of the DSC, exceeds the IAEA detection target for nuclear material accountancy.

1. Introduction

Because of their unique ability to penetrate matter, cosmic ray muons are used to image the interior of structures. Recently, a number of groups have extended the concept of muon radiography to the tracking of individual muons as they enter and exit a structure. Most current efforts have been toward demonstrating the potential for muon tomography to detect the smuggling of Special Nuclear Material (SNM) in cargo. This paper explores the application of muon tomography for non-invasive waste characterization of legacy nuclear waste containers and for nuclear material accountancy of spent fuel inside Dry Storage Containers (DSC) used to store spent CANDU® fuel.

The paper explores and reviews the concept of muon tomography and outlines how it applies to two examples of non-security related applications. This paper also presents the simulations and calculations conducted to demonstrate the efficacy of the technique and discuss the results and their implications.

2. Muon Tomography

We refer to tomography as the reconstruction of three-dimensional non-uniform matter distribution in a volume of interest from measurements made outside this volume. This differs from radiography in which only a 2-dimensional density map is obtained. In muon tomography we use the natural flux of highly penetrating cosmic-ray muons to produce images of the interior of structures.

Muons are charged particles, much like electrons, created by the interaction of cosmic radiation with the upper layer of the atmosphere. Muons have the same electric charge as electrons, which make them easy to detect but, in contrast to electrons are much more massive ($m_\mu \approx 207 m_e$) and on average have a high momentum, which confers them their strong penetrating ability. The vertical flux of energetic muons, above 1 GeV/c, at sea level is about 70 m^{-2} s^{-1} sr^{-1} (or an integrated vertical flux ≈ 1 cm^{-2} min^{-1})[1]. The mean muon energy is 3-4 GeV, which is sufficient to allow them to penetrate several meters

® Registered Trade Mark

of rock before being stopped. The idea of using muons to image large structures is not new and first measurements date from 1955. In 1970, in Egypt, Luis Alvarez dramatically demonstrated the use of cosmic-ray muons to look for hidden chambers in the Second Pyramid of Giza [2]. Muon radiographs are still in use today as a means to image structures of volcanoes in an attempt to predict volcanic eruptions [3].

These previous measurements were all based on the attenuation of the muon flux. Recently, a number of groups have extended the concept of muon radiography to the tracking of individual muons as they enter and exit structures. In muon tomography, the incoming and outgoing directions are recorded for each muon thereby producing a 3D image of the scattering location[4,5]. Multiple scattering of muons through material is mostly due to coulomb scattering from nuclei. The angular distribution of the scattered muons from a target with charge number Z is approximately Gaussian with a mean of zero and a width given by [1]:

$$\sigma_\theta = \frac{13.6MeV}{\beta cp}\sqrt{x/X_0}\left[1-0.038\ln(x/X_0)\right] \qquad (1)$$

where βc and p are the muon velocity and momentum, and x/X_0 is the material thickness in units of radiation length. Equation (1) is accurate to within 11% for $10^{-3} < x/X_0 < 100$, for all Z and with $\beta c = 1$. The Z dependence is hidden in the definition of the radiation length and for large Z, $X_0 \sim 1/Z$. Hence, the spread of scattering angles is larger for materials with high Z and small radiation length and therefore the RMS of the deflection angle of scattered muons provides a means of discriminating between low, medium and high-Z materials.

The principle of a detector system for muon tomography is shown on Figure 1. Position sensitive detectors are placed above and below the structure to be scanned (i.e. container). A minimum of two such detectors are required for each top and bottom plane such that the muon incident and exit direction can be determined. With a simple algorithm, the image is reconstructed from the Point of Closest Approach (PoCA) i.e. the point in space that is the closest to both tracks.

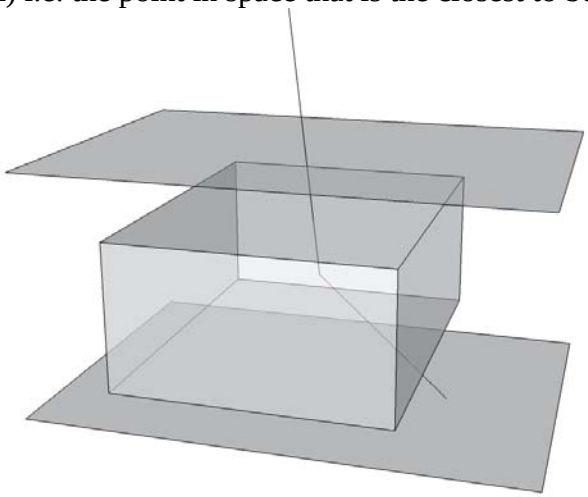

Figure 1 Concept of muon tomography: a muon enters the top detector, scatters off dense material and exits through the bottom detector planes. The reconstruction of scatter points produces a 3D image of dense scatterers.

Several methods have been proposed to discriminate further between low-Z and high-Z materials [4-8] and a number of groups have carried out developments in muon tomography. Some have focused on a system for the purpose of detecting contraband fissile material in cargo[5,6,9] while others are developing a system for tomography of canisters for spent nuclear fuel[10-12].

3. Non-security applications of muon tomography

3.1 Nuclear waste characterization

AECL maintains a radioactive waste management program to protect public health and the environment and to ensure worker safety. This is partly implemented by a program to segregate and characterize nuclear waste. Generally, radioactive waste exhibits a wide spectrum of physical, chemical and radiological characteristics, which demands a complex and tailored waste characterization program. Although, no single methodology can be adopted to treat such varied waste, strategies are beginning to emerge to develop guidance in radioactive waste characterization to facilitate long-term storage or disposal (see for example [13] and references therein). Current practice calls for establishing a process for characterizing radioactive waste during its entire life cycle which means that usually the type of waste and waste form, the evolution of the waste with time and the measurements to characterize the waste are identified upstream of segregation and disposal. Hence this is usually the case for *new wastes* as defined by those that are generated with a traceable and robust characterization program in place.

In contrast, *historical wastes* lack a comprehensive traceable characterization program which makes the process for long-term storage or disposal more difficult. In short this type of waste has a non-traceable waste stream, has incomplete history and incomplete or improper characterization. In several cases this results in a large amount of uncertainty as to the nature of the waste: origin, traceability and conditioning. This is often the case with legacy nuclear waste containers[1]. Although there is a large amount of variability of waste types and origin one can identify two components that a robust characterization program must address:

- waste complexity, which refers to the level of difficulty to develop a list of properties (*fingerprint*) to characterize the waste;
- waste stability, which refers to whether or not these properties remain relatively constant with time.

Those components refer not only to the waste content but also to the waste package. The key elements of the characterization program will involve fingerprinting the waste radioactivity, chemical, physical, mechanical, thermal and biological properties and how they evolve through time.

Challenges and issues for nuclear waste characterization are covered at great length in reference [13]. A significant subset of these is summarized below:

[1] It should be emphasised that *new* and *historical* in this context does not refer necessarily to the age of the waste i.e. nuclear waste generated today without a robust characterization program are historical waste in this IAEA classification.

- Historical waste. Non-traceable waste stream poses a challenge for characterization. Different types of waste can be distinguished: tanks with liquids, fabrication facilities to be decontaminated before decommissioning, interim waste storage sites, etc.
- Some waste form may be difficult and/or impossible to measure and characterize (i.e. encapsulated alpha/beta emitter, heavily shielded waste).
- Direct measurements, i.e. destructive assay, are not possible in many cases and Non-Destructive Assay (NDA) techniques are required which often does not provide conclusive characterization.
- Homogeneity of the waste needs characterization (i.e. sludge in tanks, in-homogeneities in cemented waste, etc.).
- Condition of the waste and waste package: breach of containment, corrosion, voids, etc.

The use of muon tomography to assist in the characterization of nuclear waste is explored further in section 4 and 5.

3.2 Non-proliferation and safeguards

Spent nuclear fuel is a form of nuclear waste with the added complexity of security and proliferation issues, and, as such, it is often placed under IAEA Safeguards. *IAEA Safeguards are measures through which the IAEA seeks to verify that nuclear material is not diverted from peaceful uses* [14]. *Traditional Measures* target the detection of diverted nuclear material. It is the historical cornerstone of safeguards and focuses on material verification activities and containment and surveillance (C/S) at facilities where the states have declared the presence of nuclear material subject to safeguards. IAEA Safeguards' item accountancy objectives are defined by the *timely* detection of a *significant amount* of nuclear material [15]. The detection targets are summarized in Table 1.

Clearly the use of muon tomography for verifying and accounting for spent fuel in dry storage is an attractive means to keep track non-invasively, remotely and unattended, of the inventory of spent fuel. In Canada, spent nuclear fuel is stored in large pools (fuel bays or wet storage) for a nominal period of 10 years to allow for sufficient radioactive cooling. Above ground dry storage is then used for the storage of used fuel. This method is considered an interim measure until an approach for long-term management of used fuel is implemented and was pioneered by AECL and Ontario Power Generation (OPG) in the mid 1970's [16,17]. These above ground facilities are essentially canisters that are used as containment to protect workers and the environment from the remnant radiation and to safeguard the spent fuel. Consequently, site storage systems must satisfy stringent safety, security and environmental requirements. The prevalent methods of dry storage are: Dry Storage Containers (DSCs) and monolithic air-cooled concrete structure for dry storage (MACSTOR – Modular Air Cooled STORage).

DSCs, such as the one shown on Figure 2, are used throughout OPG facilities. The DSC is a reinforced high-density concrete container with an inner steel liner and an outer steel shell. The DSC can store up to 384 used fuel bundles in four standard storage modules of 96 bundles each. The dimensions of the DSC are 2.12 x 2.15 m by 3.55 m height. Two stainless steel (SS) tubes are imbedded diagonally across the lid to provide for the installation of IAEA seals. Similarly, two U-shaped SS tubes are imbedded in the walls of the DSC and are used as inspection tubes by the IAEA.

Item	Quantity [kg]	Encapsulation	Time to detect diversion
U235	75	<20% enriched in NU or DU	12 months
U235	25	≥20% in HEU	1 month
Pu	8	All isotopes fresh fuel	1 month
Pu	8	All isotope spent (irradiated) fuel	3 months
U233	8	Fresh fuel	1 month
U233	8	Spent irradiated fuel	3 months

Table 1 IAEA detection targets for safeguards.

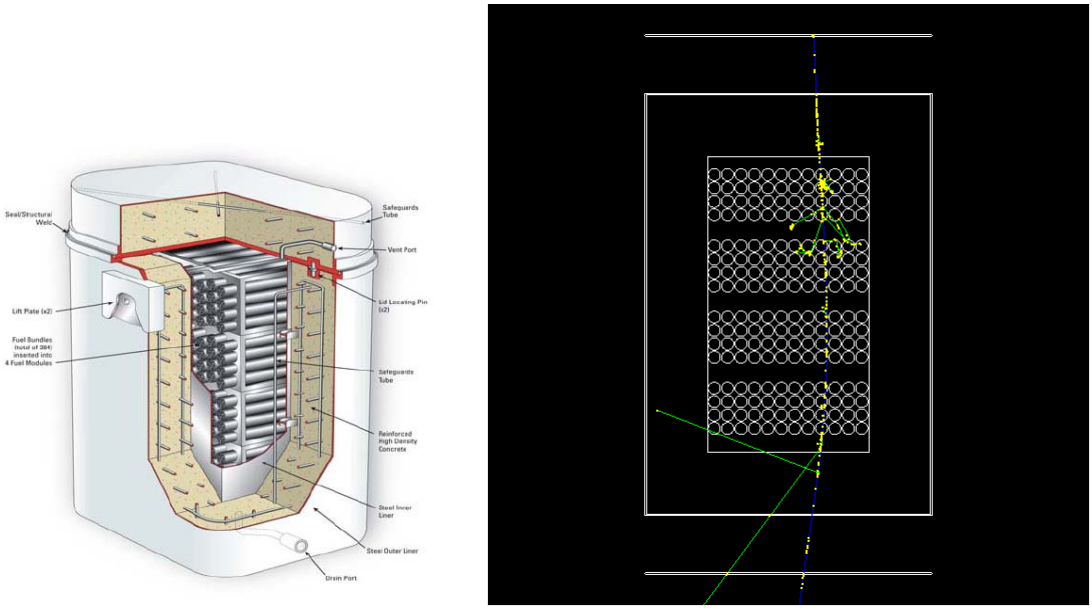

Figure 2 Cut away drawing of a Dry Storage Container (DSC) [17] **on the left and GEANT4 simulation showing a muon track and associated photons on the right.**

4. Simulations and image reconstruction

Evaluating the efficiency of muon tomography to identify nuclear materials in containers was performed by Monte Carlo (stochastic) calculations. The main advantage of performing a Monte Carlo is that it allows an event-by-event treatment so that each muon is tracked independently, as it would in a muon tomography system. Evidently, simulating the scattering of muon tracks inside containers does not in itself characterize the nuclear material detection performance of a muon tomography system. This must be addressed by image reconstruction techniques and/or statistical analysis of muon tracks.

This section describes the simulations, image reconstruction methods and derived detection performance for a selected number of container scenarios.

4.1 Simulations

Muon scattering in containers was simulated with the GEANT4 software [18]. Geant4 is a simulation toolkit designed for modeling a broad range of particle processes and their interaction with matter. It is used in a variety of applications, including High Energy Physics (HEP), nuclear physics experiment, astrophysics, space science and medical physics. Its distinguishing feature is that it allows users control over each typical domain of a simulation: geometry, particles, run, events, tracking, detector response, physics process and transparent access to cross-sections.

For the purpose of this work the detector geometry is generic and is made of two thin detector planes (trackers): one set at the top of the container and the other at the bottom. Each tracker plane is made of 1 cm thick argon at standard temperature and pressure (STP). The trackers are idealized detectors in that they register the exact muon tracking information: muon track position, direction and momentum as they cross the detection plane. Also, the trackers are made insensitive to other particles, in particular it is insensitive to track multiplicity (showers of particles) in the bottom tracker, sometimes created by high-energy muons when hitting the container. The geometry of the container volume is variable and depends on the case under study.

Only the muon component of cosmic rays has been simulated. The event generator produces muons with realistic energy and angular distribution. We used an angular distribution of muons, which is peaked at the zenith and falls off as $\cos^2\theta$, where θ is the angle from the vertical. The muon energy distribution was sampled from the BESS spectrometer data, Table 1 of reference [19]. We have used the μ^+ distribution from the 1995 measurement in Tsukuba, Japan [19], with a cut-off momentum of 0.576 GeV/c. All the most significant particle types were considered (*declared*) in the simulations (gammas, leptons, n, p and low mass mesons) but only the most significant processes were considered (for example muon capture and muon decay in-flight were neglected). Specifically for muons, multiple scattering, ionisation, bremsstrahlung and pair production were declared. Also, a threshold, below which no secondary particles will be generated, is defined during this initialization phase. This production cut parameter for the simulation was generalized for all particles as a range cut of 1 mm, which is internally converted by GEANT to an equivalent energy for different materials. There are no other tracking cuts. All particles are tracked down to the range cut. This could be relaxed later to speed-up simulations. Muons are detected as they cross the detector planes: the coordinates of the track crossings and the momentum vector are recorded. In this sense the detectors are made perfect.

4.2 Image reconstruction methods

There are several different methods of imaging high-Z material using muon tomography. We have so far arbitrarily chosen two imaging techniques: a simple Point of Closest Approach (PoCA) algorithm and the Maximum Likelihood/Expected Maximization (ML/EM) tomographic reconstruction algorithm as described in reference [20,21]. This latter method exploits, in addition to the tracks directions, the muons momentum information. The ML/EM method was used with a slightly different approach in the scattering strength distribution of voxels.

4.2.1 Point of closest approach (PoCA)

The PoCA method is used to approximate the point of scattering of muons through container volumes. One can assume that the scattering occurred due to a single scattering event and locate that point by extrapolating the incident ($\boldsymbol{\mu}_1$) and outgoing muon trajectory ($\boldsymbol{\mu}_2$) to their PoCAs. Hence each muon track is defined by $\mathbf{r}$ and $\mathbf{q}$ where $\mathbf{r}$ is the coordinate of the muon trajectory crossing a tracker plane and $\mathbf{q}$ the momentum vector of the trajectory. The PoCA on each trajectory are then easily computed from the line equations:

$$\boldsymbol{\mu}_1(s) = \mathbf{r}_1 + s\mathbf{q}_1 \text{ and } \boldsymbol{\mu}_2(t) = \mathbf{r}_2 + t\mathbf{q}_2, \quad (2)$$

evaluated at the PoCAs, where *s* and *t* are scalar parameters. The point of scattering is given as the midpoint between the two PoCAs. Plotting these points in itself does not usually reveal high Z materials since muons will also scatter in the surroundings. Normally additional cuts are needed on the scattering angle at the expense of reducing the data sample size.

4.2.2 Maximum Likelihood/Expected Maximization (ML/EM) tomographic reconstruction algorithm

The ML/EM tomographic reconstruction method, as described in references [6] and [20], was also implemented as a measure against the PoCA technique. The method uses as input the positions and momenta for each muon on the top and bottom surfaces of the volume of interest and considers the probability function of the measured scattering against the scattering angle of each muon in voxels within the volume under scrutiny. We refer the reader to reference [6] for additional details. We have modified the definition of the scattering segments in the scattering strength. This work will be described in future publications.

5. Results and discussions

5.1 Waste characterization

The diversity of nuclear waste characteristics makes it unrealistic to look at all possible scenarios where muon tomography can be used to characterize waste; however an example is chosen to illustrate the potential of this technology. This example is tailored to the potential advantages of muon tomography: NDA capability, sensitivity to atomic number, and the capability to image the content and the structure of the containers. The following case has been analyzed: fuel pencil (10 cm long, 1 cm diameter UO_2) encapsulated in a 55-gallon stainless steel drum. The drum is filled with paraffin. A 10 cm diameter void has also been added to simulate breach of containment.

The fuel pencil was positioned parallel with the central axis of the drum but some distance away from the centre. One day's worth of cosmic ray muons was originally generated or about 400 000 events. Figure 3 shows a 2D projection of the canister using the EM/ML reconstruction algorithm. The pin location is very prominent.

Implicit in the use of this technology is the ability to detect a small, high-density scatterer. Work is ongoing to assess how the waste content can be further characterized beyond imaging material densities.

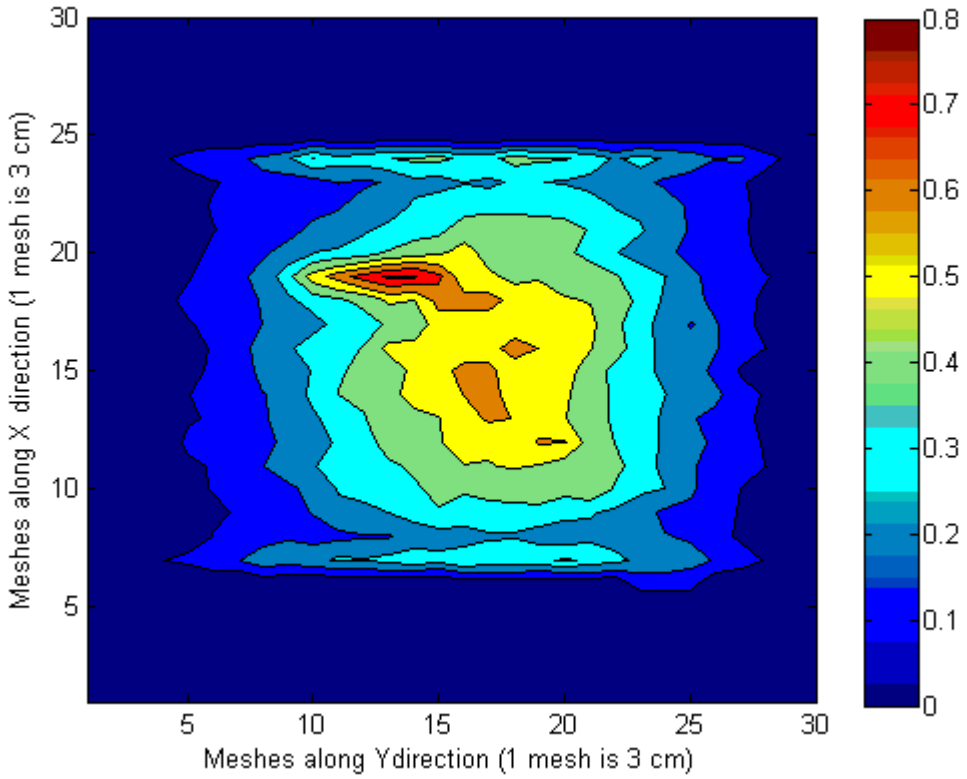

Figure 3 ML/EM reconstructed image of a UO_2 fuel pin inside a stainless steel drum on its side.

5.2 Spent fuel monitoring results

The problem of monitoring spent fuel in DSCs, using muon tomography, is vastly different than that of waste characterization. First, the container under scrutiny is assumed well known and one looks for deviations from a known configuration. Secondly, the safeguards requirements of timely detection and significant quantity (see Table 1) are generally less stringent than contraband detection and a significant amount of data can be acquired to draw conclusions. Thirdly, the assumption of a single scattering point can no longer be used owing to the large amount of spent fuel gathered together. Therefore the image reconstruction techniques devised so far fail to produce meaningful images.

To evaluate the ability of muon tomography to safeguard spent fuel, we have simulated a single type of spent fuel container modelled after the DSC with some simplifications. Figure 2 right shows a cut away view of the simulated geometry. The model contains the same number of CANDU fuel bundle as a full DSC: 384 used fuel bundles in four standard storage modules of 96 bundles each. Each row is 2 bundles in length. The walls of the DSC were modelled as a concrete (density 2.3 g/cm^3) box of dimensions 2.12 m x 2.15 m by 3.55 m height with a wall thickness of 52 cm. The concrete is surrounded by a thin, 1.3 cm, carbon steel shell (density 7.87 g/cm^3).

Figure 2 also illustrates a typical muon event. The extent of the continuous scattering and the large number of multiple interactions, visible through secondary particles, of the muon with the fuel and the concrete is apparent in the figure. Muons typically lose about 1 GeV while going through the DSC and so a large fraction of the muons are stopped before reaching the bottom detector plane. As is evident from the figure, the continuous scattering of the muon coupled with the homogeneity of materials does not permit one to define a single scattering point. Previous trials showing the PoCAs distribution for

two stringent angular cuts of 5° and 20° have showed that fuel bundles cannot be distinguished in the picture.

Although the muon tomography methods described cannot be used to construct an image of large amounts of dense material, muon radiography is expected to show density variations. Figure 4 shows a radiograph of a DSC with 2 columns of fuel missing. Our earlier attempts at producing muon radiographs from flux measurements of outgoing muons did not produce flux profiles from which an accurate density plot could be produced. This was attributed to the $\cos^2\theta$ angular distribution of muons and hence the large differences in scattering strength for muons recorded in similar area of the bottom detector plane. A flux profile was then built from counting only through-going muons. The accounting was performed by registering only muons which passed through overlapping vertical regions: a muon is registered if it recorded a hit in a top region (cell) and a bottom cell directly on top of each other. Effectively, this method amounts to imaging the effect of the container on a parallel beam of muons. Figure 4 shows the radiograph obtained for the case with 5 cm x 5 cm cells. The green lines indicate actual location of fuel bundles. The central region, where fuel bundles are missing, shows a much higher muon flux and is clearly discernable along with the concrete walls and the fuel bundles. This radiograph was produced with 12 Million muons or 1 day equivalent. About 48,000 muons pass the cuts described above or 0.4 %.

To further quantify the efficiency of muon radiography in meeting IAEA Safeguards' item accountancy objectives, a DSC container with 2 contiguous fuel bundles removed, or one row, was simulated (as opposed to the 4 entire columns of missing fuel in Figure 4). In this simplified model, each fuel bundle is a simplified full cylinder and so the bundle's total mass of UO_2 is about 40kg. Assuming about 0.35 wt % U235 and the same amount of Pu239 in spent bundles, this represents a total content[2] per bundle of about 0.15 kg of U235 and 0.15 kg of Pu239. Muon radiographs (parallel beam method) were obtained from a simulation of 9 days worth of muons (107 Million muons) of which 308 000 remain after cuts (0.3 %). In this analysis, a 11.3 cm cell size along the x-axis and a 8.4 cm cell size along the z-axis was used. The cell size was chosen such that a number of integral cells covered the fuel bundles.

Figure 5 shows the muons counts projected on one axis of the radiograph. The high point, at position $x = 17$ cm where 2 bundles are missing, shows 26962 ± 164 counts, which is 5σ away from the mean, indicated by the orange line on Figure 5. Therefore, within 9 days, muon flux measurements on a DSC could be sensitive to a loss of 2 bundles with a high degree of confidence. Although, the flux radiograph on its own is not able to separately identify actinide content, it is likely that this kind of measurements compared with expected attenuation of muons as a function of material density, will provide a way to perform non-invasive material accountancy of nuclear materials with a high degree of confidence that greatly exceed the IAEA detection targets as shown in Table 1. Note that the low points at the extremities of the graph in Figure 5 are explained by edge effects. Muons which scatter in edge bundles and in the concrete have a smaller probability of re-entry into the bundle column where flux is being computed.

[2] CANDU bundle are in reality closer to 20 kg total weight. This simplified model will be extended in the future to more realistic bundle geometry. This simplification does not modify the general conclusions.

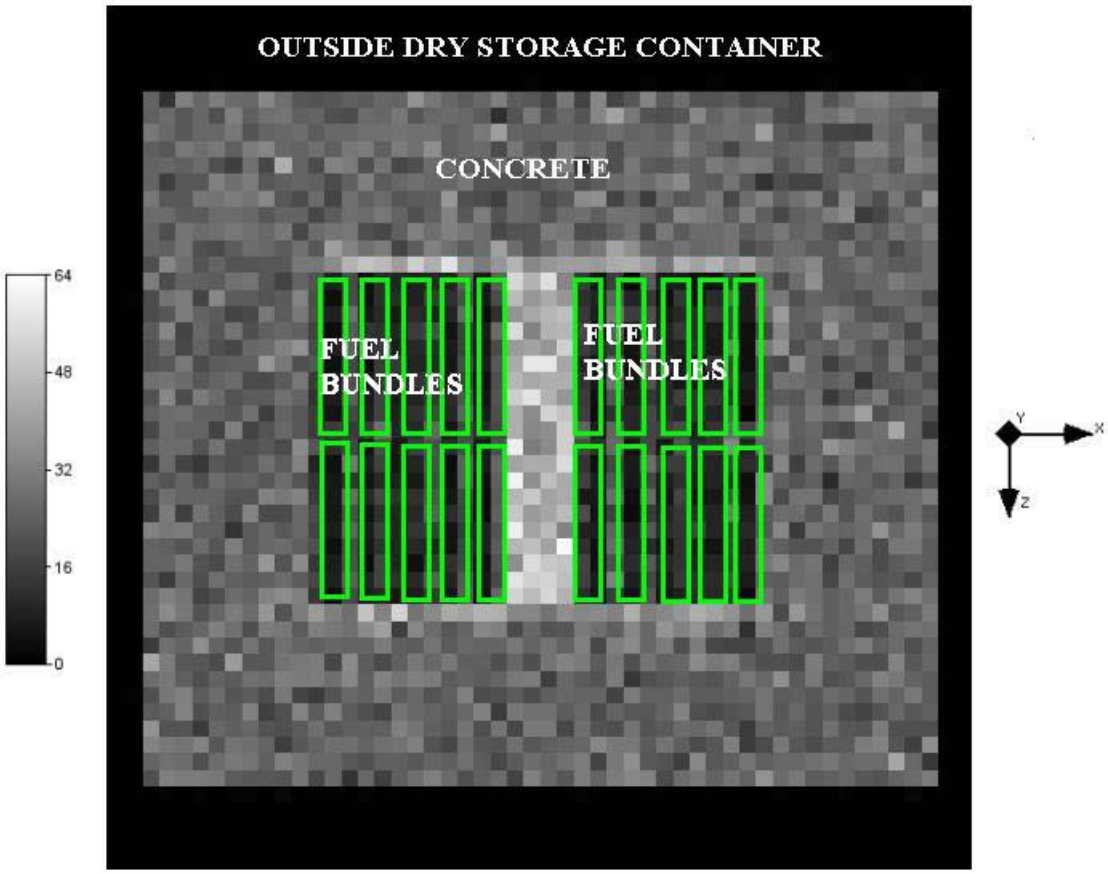

Figure 4 A Dry Storage Container

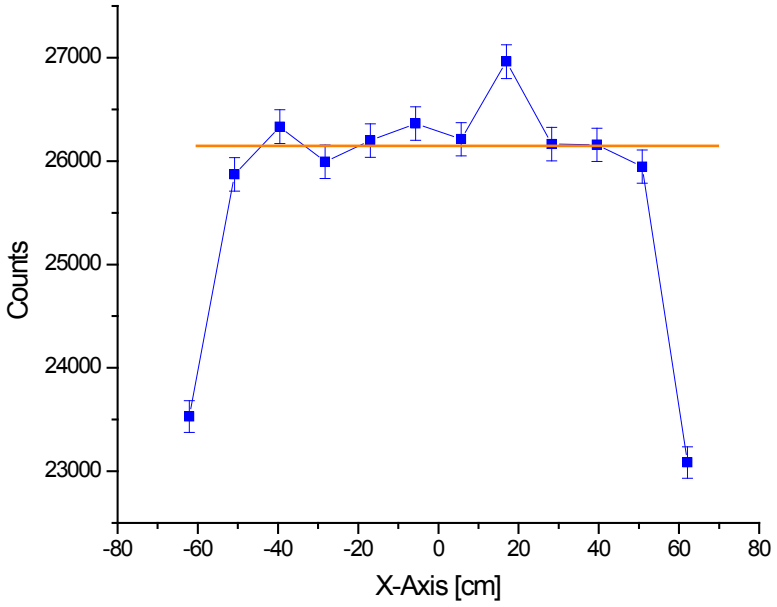

(DSC).

Figure 5 Muon flux (arbitrary units) projected along one DSC axis.

6. Conclusion

This paper outlined the potential application of a muon tomography device for non-security related applications. Muon tomography holds much potential for non-invasive nuclear material accountancy of dry storage containers in that it can potentially improve the accuracy and availability of data on the content of dry storage containers. This can be achieved non-invasively, with the potential for unattended and remotely monitored operation. We have shown that the expected sensitivity to perform material accountancy, in the case of the DSC, greatly exceeds the IAEA detection target for non-proliferation and safeguards.

Owing to the diversity of nuclear waste, it is somewhat unrealistic to look at all possible scenarios where muon tomography can be used to characterize waste. However, we have shown, through one example, that the method may be useful in identifying clumps of actinides in shielding containers.

Future work will investigate the application of the method to characterize sludge precipitation in radioactive liquid waste containers and breach of containment.

7. Acknowledgements

The authors whish to acknowledge Bhaskar Sur for suggesting the use of muon tomography as a means to characterize nuclear waste and also for many useful discussions.

8. References

[1] C. Amsler *et. al.*, Particle Data Group, "Review of particle physics", *Physics Letters* B 667 (2008) 1.

[2] L. W. Alvarez, *et. al., Science* 167 (1970) 832.

[3] K. Nagamine, *J. Geogr.* 104 (1995) 998.

[4] M. Österlund *et. al.*, International Workshop on Fast Neutron Detectors and Applications, Cape Town, South Africa, April 3-6, 2006.

[5] L.J. Schultz, *et. al.*, "Cosmic ray muon radiography for contraband detection", *Proceeding of AccApp'03*, San Diego, CA, June 2003

[6] L.J. Schultz *et. al.*, *Nucl. Instr. Meth.* A519 (2004) 687.

[7] W. C. Priedhorsky, *et. al., Rev. Sci. Instr.* 74 (10) (2003) 4294

[8] J.A. Green, *et. al.*, "Optimizing the tracking efficiency for cosmic ray muon tomography", 2006 IEEE Nuclear Science Symposium Conference, LA-UR-06-7556 (2006).

[9] K. Borozdin, *et. al., Nature* 422 (2003) 277.

[10] J. Donnard, Rapport de synthèse, Departement of Neutron Res., Uppsala University, Internal Report (2004).

[11] A. Flodin, "Cosmic muons for the detection of high-Z materials", Uppsala University, INF, UU-NF05 #4 (2005).

[12] J. Gustafsson, “Tomography of canisters for spent nuclear fuel using cosmic-ray muons”, Uppsala University, INF, UU-NF05 #8 (2005).

[13] IAEA Report, “Strategy and methodology for radioactive waste characterization”, IAEA-TECDOC-1537, March 2007.

[14] IAEA Department of Safeguards, “IAEA safeguards: staying ahead of the game”, Printed by the IAEA, July 2007.

[15] IAEA, “Design measures to facilitate the implementation of safeguards at future water cooled nuclear power plants”, IAEA Technical Report Series 392, STI/DOC/010/392, January 1999.

[16] Frost, *et. al.*, “Current interim used fuel storage practice in Canada”, Used Fuel Management Engineering Department, Ontario Hydro, Report No. N-03710-940052, June 1 1994.

[17] Nuclear Waste Management Organization (NWMO) Background Paper, “Technical Methods”, SENES Consultant Limited, 33532-FINAL, October 2003.

[18] GEANT4 Collaboration, “GEANT4 users’s guide for application developers”, Version geant4 9.1, Published 14 December 2007.

[19] M. Motoki et. al., “Precise measurements of atmospheric muon fluxes with the BESS spectrometer”, *Astropart. Phys.*, 19 (2003), 113-126.

[20] L. J. Schultz *et. al.*, “Statistical reconstruction for cosmic ray muon tomography”, *IEEE transaction on image processing*, Vol. 16, No. 8, August 2007.

[21] L. Schultz, G. Blanpied, K. Borozdin, A. Fraser, A. Klimenko, N. Hongartner, C. Morris, C. Orum, M. Sossong, “ML/EM reconstruction algorithm for cosmic ray muon tomography”, IEEE Nuclear Science Symposium, 2006.